Title

Porcupine Inhibition Disrupts Mitochondrial Function and Homeostasis in WNT Ligand-Addicted Pancreatic Cancer.

Journal

Molecular Cancer Therapeutics, 21(6)

ISSN

1535-7163

Authors

Aguilera, Kristina Y
Le, Thuc
Riahi, Rana
et al.

Publication Date

2022-06-01

DOI

10.1158/1535-7163.mct-21-0623

Peer reviewed

HHS Public Access

Author manuscript

Mol Cancer Ther. Author manuscript; available in PMC 2022 December 01.

Published in final edited form as:

Mol Cancer Ther. 2022 June 01; 21(6): 936–947. doi:10.1158/1535-7163.MCT-21-0623.

Porcupine inhibition disrupts mitochondrial function and homeostasis in WNT ligand-addicted pancreatic cancer

Kristina Y. Aguilera[1], **Thuc Le**[2,3], **Rana Riahi**[1], **Anna R. Lay**[1], **Stefan Hinz**[4], **Edris A. Saadat**[1], **Ajay A. Vashisht**[5], **James Wohlschlegel**[5], **Timothy R. Donahue**[1,2,3,6], **Caius G. Radu**[2,3], **David W. Dawson**[1,7]

[1]Department of Pathology and Laboratory Medicine, David Geffen School of Medicine, University of California, Los Angeles, CA, 90095.

[2]Department of Molecular and Medical Pharmacology, University of California, Los Angeles, CA, 90095.

[3]Ahmanson Translational Imaging Division, University of California, Los Angeles, CA, 90095.

[4]Department of Population Sciences, Beckman Research Institute, City of Hope, Duarte, CA 91010, USA.

[5]Department of Biological Chemistry, University of California, Los Angeles, Los Angeles, CA, 90095.

[6]Department of Surgery, University of California, Los Angeles, CA, 90095.

[7]Jonsson Comprehensive Cancer Center, David Geffen School of Medicine, University of California, Los Angeles, CA, 90095.

Abstract

WNT signaling promotes pancreatic ductal adenocarcinoma (PDAC) through diverse effects on proliferation, differentiation, survival, and stemness. A subset of PDAC with inactivating mutations in *ring finger protein 43 (RNF43)* show growth dependency on autocrine WNT ligand signaling and are susceptible to agents that block WNT ligand acylation by Porcupine O-acyltransferase, which is required for proper WNT ligand processing and secretion. For this study, global transcriptomic, proteomic, and metabolomic analyses were performed to explore the therapeutic response of *RNF43*-mutant PDAC to the Porcupine inhibitor (PORCNi) LGK974. LGK974 disrupted cellular bioenergetics and mitochondrial function through actions that included rapid mitochondrial depolarization, reduced mitochondrial content, and inhibition of oxidative phosphorylation and tricarboxylic acid cycle. LGK974 also broadly altered transcriptional activity, downregulating genes involved in cell cycle, nucleotide metabolism, and ribosomal biogenesis and upregulating genes involved in epithelial-mesenchymal transition, hypoxia, endocytosis, and lysosomes. Autophagy and lysosomal activity were augmented in response to LGK974, which

Corresponding author: David W. Dawson, M.D., Ph.D., [1]Department of Pathology and Laboratory Medicine, [5]Jonsson Comprehensive Cancer Center, David Geffen School of Medicine, University of California, Los Angeles, CA, 90095, 310-825-0618, DDawson@mednet.ucla.edu.

Conflict of interest statement

There are no potential conflicts of interest

synergistically inhibited tumor cell viability in combination with chloroquine. Autocrine WNT ligand signaling dictates metabolic dependencies in *RNF43*-mutant PDAC through a combination of transcription dependent and independent effects linked to mitochondrial health and function. Metabolic adaptations to mitochondrial damage and bioenergetic stress represent potential targetable liabilities in combination with PORCNi for the treatment of WNT ligand-addicted PDAC.

Introduction

Pancreatic ductal adenocarcinoma (PDAC) is the third leading cause of cancer mortality in the United States and is characterized by its advanced stage at clinical presentation, biological aggressiveness, and therapeutic resistance (1, 2). WNT signaling promotes pancreatic tumor initiation, progression, dissemination, and therapeutic resistance by regulating cellular proliferation, differentiation, survival, stemness/pluripotency, and metabolism (3–9). Canonical WNT signaling is initiated by the oligomerization of WNT ligand, frizzled (FZD) receptor, and low-density lipoprotein-receptor related protein 5/6 (LRP5/6) that results in the stabilization and nuclear translocation of β-catenin where it mediates target gene expression (8).

Of therapeutic interest is a subset of PDAC (5–7%) with inactivating mutations in *ring finger protein 43* (*RNF43*), a transcriptional target and feedback inhibitor of canonical WNT signaling that occurs by ubiquitination and clearance of FZDs. Inactivating mutations in *RNF43* increase WNT ligand-mediated signaling through FZD-LRP5/6 (Figure 1A) (9). *RNF43*-mutant PDAC demonstrate constitutive autocrine WNT ligand/β-catenin transcriptional activity, growth dependency on autocrine WNT ligand signaling, and responsiveness to inhibitors of WNT ligand-FZD receptor signaling, including small molecule inhibitors of Porcupine (PORCNi) (9, 10). Porcupine is an endoplasmic reticulum membrane protein that O-palmitoleoylates WNT ligands, a post-translational modification required for proper WNT ligand processing, secretion, and receptor binding activity. The PORCNi LGK974 and ETC-159 antagonize the *in vitro* and *in vivo* growth of WNT ligand-addicted tumors via their inhibition of PORCN and autocrine WNT signaling activity (11, 12) and share a common mechanism of action of docking in the PORCN catalytic site (13, 14). Several PORCNi (LGK974, ETC-159, CGX1321, and RXC004) with similar pharmacokinetics and pharmacodynamics have advanced to clinical trials based on their favorable properties, exquisite potency, and specificity in inhibiting WNT ligand secretion and signaling (15, 16).

RNF43 mutations promote β-catenin transcriptional activation but will also augment signaling events upstream of β-catenin and the APC/AXIN/GSK3β/CK1 destruction complex, including enhanced WNT-FZD-LRP5/6 activation that is linked to the formation of endocytic LRP6 signalosomes. LRP6 signalosomes sequester GSK3β (glycogen synthase kinase 3 beta) to prevent it from phosphorylating proteins and targeting them for proteasomal degradation (17, 18). GSK3β sequestration has the potential to impact its biochemical activity, subcellular localization, and/or protein interactions of various substrates regulated by its phosphorylation (19).

Here an unbiased multi-omic approach exploring the global effects of PORCNi has uncovered a novel role for autocrine WNT ligand signaling in the maintenance of mitochondrial function and homeostasis in *RNF43*-mutant PDAC. PORCNi led to rapid mitochondrial depolarization and increased localization of active GSK3β to mitochondria. Autophagy was also increased, which could be targeted pharmacologically with chloroquine in combination with LGK974 to inhibit *in vitro* cell viability synergistically. This study highlights an underappreciated link between autocrine WNT ligand signaling and mitochondrial homeostasis and function in regulating the bioenergetic and biosynthetic growth demands of WNT-addicted PDAC.

Materials & Methods

Cell lines and antibodies

Human PDAC cell lines AsPC-1, HPAF-II, Capan-2, MIA PaCa-2, PANC-1, T3M-4, SU.86.86, and Panc 02.03, and HPDE (an immortalized, non-transformed pancreatic ductal epithelial cell line) were cultured in DMEM, RPMI, or McCoy's 5A media (Invitrogen) with 10% fetal bovine serum (VWR). Control and Wnt3a conditioned media (CM) were collected as described from control murine L-cells or L-cells expressing *Wnt3a* (4). All cell lines were authenticated by short tandem repeat testing and tested mycoplasma free. See Supplemental Table 1 for additional information.

Drugs and reagents

Drugs (Cayman Chemical) were used, unless otherwise indicated, at 25 nM LGK974 (#14072), 10 μM carbonyl cyanide 3-chlorophenylhydrazone (CCCP, #25458), 20–40 μM chloroquine (#30708), and 20 nM Bafilomycin A1 (#11038). Trypan blue (MT25900CI), DMSO (D136–1), and Prolong Gold with DAPI (P36941) from Fisher Scientific, Hoechst solution (33342) purchased from Thermo Fisher Scientific, and DeadEnd FL TUNEL System (G3250) from Promega.

Immunoblots

Mitochondrial extracts were collected with Qproteome mitochondria isolation kit (Qiagen 37612). Triton-X 100 whole cell lysates and mitochondrial lysates were resolved by SDS-PAGE and transferred to PVDF membranes. Membranes were blocked for 1 hour in 5% BSA in TBS-T, incubated with primary antibody overnight at 4°C, washed with TBS-T, incubated 1-hour with HRP-conjugated secondary antibody, washed, and imaged using enhanced chemiluminescence reagent (ECL, Super Signal West Pico PLUS Luminol/ Enhancer, Fisher Scientific) with Odyssey Fc (Li-Cor). Individual bands were quantified and normalized using ImageStudioLite (LI-COR RRID:SCR_013715).

Gene Silencing

CTNNB1 siRNA (Target sequence GGATGTTCACAACCGAATT, Integrated DNA Technology), Thermo Fisher Scientific Stealth siRNA Negative Control (12935200), or siRNA *WNT7B* (pooled HSS111365 and HSS111366) were transfected at 5 nM using Lipofectamine 2000 reagent (Invitrogen). >70% gene knockdown confirmed by qPCR (Supplemental Figure 4A).

Flow cytometry

Measures of cell cycle by propidium iodine (Abcam, ab14085) or mitochondrial membrane potential (MMP) by MitoProbe JC-1 (Thermo Fisher Scientific, M34152) with BD LSRFortessa (BD Biosciences) flow cytometer and FlowJo version 10 software (RRID:SCR_008520).

Metabolite production/consumption assays

Conditioned cell media were collected and processed using Lactate-Glo (J5021), Glucose-Glo (J6021), or Glutamine/Glutamate-Glo (J8021) per manufacturer's (Promega) instructions with data normalized to live cell counts determined at media collection.

Seahorse assays

Seahorse XF microplate analyzer assessment of oxygen consumption rate (OCR) and extracellular acidification rate (ECAR) of whole cells or mitochondria. Addition of reagents is well-described (20). Data was normalized to number of viable cells or mitochondria, respectively.

Biosensor and immunofluorescence assays

Equal numbers of viable cells were determined by trypan blue exclusion processed per manufacturer's instructions (Thermo Fisher Scientific) with tetramethylrhodamine methyl ester perchlorate (TMRM, T668), MitoTracker Green-FM (M7514), and LysoSensor Green-DND-189 (L7535) and visualized by immunofluorescence microscopy and/or plate reader. For immunocytochemistry, cells were fixed and stained with HRP-conjugated primary antibodies, followed by FITC and TRITC-labeled secondary antibodies. Images ($n > 6$) were captured with Olympus EX41 microscope and Olympus DP Controller software (Olympus Life Science) with Fiji software (V2.0.0) (RRID:SCR_002285) quantification. FUW mCherry-GFP-LC3 plasmid (RRID:Addgene_110060) was transfected in HEK293 (RRID:CVCL_0045) to generate lentiviral particles used to stably transduce AsPC-1 using Bleocin selection.

ATP levels

Equal numbers of viable cells were determined by trypan blue exclusion were measured by CellTiterGlo3D (Promega, G9681).

Metabolomics

^{13}C metabolic mass isotopomer distribution analysis (MIDA) via labeled glucose was used to quantitatively evaluate incorporation into various metabolites. Data was normalized to protein content by BCA assay based on the median protein content of three biological replicates for each treatment group. Analysis was performed on a Q Exactive (Thermo Fisher Scientific) in polarity-switching mode with positive voltage 4.0 kV and negative voltage 4.0 kV. Mass spectrometer was coupled to an UltiMate 3000RSLC (Thermo Scientific) UHPLC system. Metabolites were detected and quantified as area under the curve based on retention time and accurate mass (≤ 3 p.p.m.) using the TraceFinder 3.1 (Thermo Fisher Scientific). Relative amounts of metabolites between various conditions, as well as

percentage of [^{13}C6] glucose labelling, were calculated and corrected for naturally occurring ^{13}C abundance.

Transcriptomics

RNA sequencing libraries were constructed from total RNA using the KAPA Stranded mRNA kit and sequenced on an Illumina Hi Seq 3000 using the Hi Seq 3000/4000 SBS kit (50 cycles). Raw reads were aligned to the UCSC Human Genome hg19 using the Bowtie2 aligner (version 2.2.9) (RRID:SCR_016368). Read count was performed by RSEM (version 1.2.25) (RRID:SCR_013027). Genes with less than 10 fragments in all samples were excluded from differential expression analysis determined using the DEseq2 pipeline (version 2.6.10) (RRID:SCR_015687). FDR cutoff of < 0.05 was considered significant. Gene set enrichment analysis (GSEA, v2.2.3) (RRID:SCR_003199) was performed on ranked lists of differentially expressed genes using the GSEAPreranked tool and Hallmark, C2:CP:KEGG gene set categories obtained from the Molecular Signatures Database. Default GSEA parameters were used with the exception of the classic enrichment statistic.

Stable isotope labeling by amino acids in cell culture (SILAC)

AsPC-1 maintained in “heavy” media containing $^{13}C_6$ L-lysine-2HCl and 50mg of L-arginine-HCl or “light” media containing L-lysine-2HCl and 50mg of L-arginine-HCl in DMEM (Thermo Fisher Scientific, 89985) were treated. Denatured protein extracts were trypsinized, fractionated by reversed phase peptide chromatography, and analyzed by LC-MS/MS on a Q-Exactive mass spectrometer (Thermo Fisher Scientific) as previously described (21). Data was analyzed by IP2 informatics platforms in which (1) the SEQUEST database searching algorithm was used to match peptide sequences to MS/MS spectra, (2) the DTASelect algorithm was used to filter peptide and protein identifications at a decoy database-estimated false positive rate of 1%, and (3) Census was used for relative quantitation of SILAC pairs between control and treated samples.

HSA and Loewe synergy analysis

Synergy analyses were performed using synergyfinder (V 2.4.10) (RRID:SCR_019318) R package available through Bioconductor. Cell viability responses and drug treatment concentrations were utilized to calculate the synergy score using the CalculateSynergy function for Loewe and HSA methods (22).

Data availability

RNA-seq transcriptomics data is deposited on Gene Expression Omnibus (GEO), accession number GSE180615. Metabolomics data is deposited on Metabolomics Workbench, study ID ST001902.

Statistical analysis

Statistical analysis was performed using GraphPad Prism 7.0 (GraphPad Software) (RRID:SCR_002798). Statistics: Student’s T-Test or One-way ANOVA (*, $p \leq 0.05$; **, $p \leq 0.01$; ***, $p \leq 0.001$; ****, $p \leq 0.0001$) with all values expressed as mean ± SEM of

biological replicates. Presented data is a representative assay of experiments conducted a minimum of three times with 3–5 biological replicates per condition.

Results

PORCNi inhibits growth of *RNF43*-mutant PDAC by impacting gene and protein expression

Consistent with previous studies (3, 4, 10, 23), low nanomolar concentrations of LGK974 inhibited β-catenin/TCF-dependent transcriptional activity of various PDAC cell lines, but only inhibited the growth and viability of lines harboring *RNF43* mutations (AsPC-1, HPAF-II, and Capan-2) in anchorage dependent (AD) and anchorage independent (AI) growth assays (Supplemental Figure 1A–D). LGK974 growth inhibition was attributable to reduced cell proliferation associated with G1 cell cycle arrest (Figure 1B–C, Supplemental Figure 1E), as well as increased apoptosis (Figure 1D, Supplemental Figure 1F) with cleaved caspase 3 and cleaved PARP increased to levels similar to that induced by the potent oxidative phosphorylation uncoupling agent carbonyl cyanide 3-chlorophenylhydrazone (CCCP) (Figure 1E–F, Supplemental Figure 1G).

To identify mechanisms underpinning growth inhibition by LGK974, RNA sequencing with differential gene expression analysis was performed at multiple time points in AsPC-1 (Supplemental Figure 1H, Supplemental Table 2, Figure 1G). Few genes were altered at 4 hours (adjusted, $p<0.05$) including subtle downregulation of established targets of canonical WNT signaling—*AXIN2, MYC,* and *BMP4* (−0.11, −0.21, and −0.24 log2 fold change, respectively). Widespread transcriptional alterations occurred at 24 and 72 hours (~15% and ~22% of expressed genes, respectively, adjusted $p<0.05$), including multiple targets of canonical WNT signaling (Supplemental Figure 1H, Supplemental Table 2), consistent with a recent *in vitro* and *in vivo* temporal study of transcriptomic alterations mediated by ETC-159 (3). A comparison of 25 nM versus 1 μM LGK974 at 24 hours revealed very few differences in gene expression (18 altered genes, adjusted $p<0.05$), indicating LGK974 transcriptional effects are specific even at concentrations well beyond that needed to potently inhibit WNT ligand secretion.

The most significant KEGG and Gene Ontology (GO) terms in gene set enrichment analysis (GSEA) included negative enrichment of spliceosome, DNA replication, cell cycle, purine and pyrimidine metabolism, NCRNA metabolic processes, and ribosomal biogenesis (Figure 1G). Negatively enriched E2F and MYC target Hallmark terms were consistent with cell cycle arrest and rapid transcriptional downregulation of *MYC.* Positively enriched GSEA terms included hypoxia, endocytosis, lysosome, process utilizing autophagic mechanism, endocytosis, and vesicle transport (Figure 1G), well established adaptive responses to cellular and metabolic stress. A comparative analysis of a publicly available RNA-seq dataset of orthotopic HPAF-II tumors treated *in vivo* with ETC-159 (3) revealed a highly similar enrichment of gene set terms (Supplemental Figure 2A–B), supporting the biological significance of *in vitro* transcriptomic analyses with LGK974 here.

Unbiased quantitative proteomic mass spectrometry analysis by stable isotope labeling by amino acids in cell culture (SILAC) was performed to identify potential post-translational alterations mediated by PORCNi treatment in WNT-addicted PDAC (Figure 2A–B).

LGK974 versus control treated AsPC-1 were compared at 8 hours when inhibition of LRP6 phosphorylation begins to peak (Supplemental Figure 3). Significant changes were detected at this early time point, including 642 downregulated proteins and 115 upregulated proteins (absolute fold change >0.33, adjusted $p<0.05$, Supplemental Table 3). Multiple mitochondrial and ribosomal GO terms were negatively enriched (Figure 2A). KEGG terms negatively enriched included oxidative phosphorylation, as well as Parkinson, Alzheimer, and Huntington diseases, neurodegenerative disorders with pathophysiologic links to mitochondrial dysfunction (24). Mitochondria-associated proteins were amongst the most downregulated (Figure 2B), some but not all of which were transcriptionally downregulated (e.g., *TFAM* and *OPA1*) at 24H.

PORCNi disrupts mitochondrial homeostasis in *RNF43*-mutant PDAC

Mitochondrial proteins were significantly downregulated in the SILAC analysis. LGK974 effects on mitochondrial status and function were examined across *RNF43*-mutant PDAC cell lines. LGK974 decreased mitochondrial content by western blot for mitochondrial matrix protein TOM20 levels and MitoTracker Green fluorescence imaging (Figure 2C–D, Supplemental Figure 4B). LGK974 also decreased mitochondrial membrane potential (MMP) measured by tetramethylrhodamine methyl ester (TMRM) and JC-1 assays (Figure 2E–F, Supplemental Figure 4C). MMP (2–4 hours) was decreased prior to changes in mitochondrial content (4–8 hours) at a magnitude and kinetics similar to those observed with the potent oxidative phosphorylation uncoupling agent CCCP (Figure 2G, Supplemental Figure 4D). Downregulation of MMP and mitochondrial content by LGK974 were reversed with the addition of exogenous Wnt3a ligand (Figure 2H, Supplemental Figure 4E) and were phenocopied by *WNT7B* siRNA knockdown (Figure 2I, Supplemental Figure 4A). *WNT7B* was previously shown to be required for autocrine WNT signaling activity and growth of *RNF43*-mutant PDAC cell lines (4, 23). LGK974 had no effect on the mitochondria of wild-type *RNF43* PDAC cell lines or the non-transformed pancreatic ductal cell line HPDE (Supplemental Figure 4F). These results indicate inhibition of autocrine WNT ligand signaling by LGK974 rapidly disrupts MMP and mitochondrial homeostasis specifically in *RNF43*-mutant PDAC.

Mitochondrial depolarization occurs with prolonged opening of the mitochondrial permeability transition pore (mPTP), a high conductance mitochondrial membrane channel of debated structural and regulatory components. Among established regulators of the mPTP is mitochondrial matrix-localized peptidyl-prolyl cis–trans isomerase cyclophilin-D (CyP-D). Cyclosporin A (CsA) directly binds CyP-D to inhibit mPTP formation (25). CsA blocked mitochondrial depolarization induced by LGK974 (Figure 3A), indicating LGK974 disrupts MMP through a mechanism linked to the mPTP. Pro-oncogenic signaling pathways are known to regulate various mitochondrial phenotypes, including MMP and oxidative phosphorylation, through the phosphorylation and inhibition of basal GSK3β activity. Active GSK3β phosphorylates mPTP regulatory components to lower mPTP threshold. It also mediates indirect effects that shift the balance of inducing/inhibitory factors in the mitochondrial matrix that trigger pore transition (25–32). Examining GSK3β further, total levels of GSK3β and its Ser 9 phosphorylated inactive form (P-GSK3β-Ser9) were unchanged in whole cell lysates following LGK974 treatment (Supplemental Figure 5). In

contrast, LGK974 significantly increased the localization of active GSK3β to mitochondria as evidenced by an increase in total GSK3β in parallel with a decrease in its inactive P-GSK3β-Ser9 form in isolated mitochondrial extracts (Figure 3B). Thus, LGK974 increased the localization of active GSK3β to mitochondria where it has a known role in lowering mPTP threshold and triggering pore transition.

Mitochondrial homeostasis is coordinately regulated through mitochondrial biogenesis, dynamics, and clearance via autophagy (mitophagy). Stabilization of PINK1 on the outer mitochondrial membrane (OMM) promotes mitophagy by phosphorylating PARKIN and other substrates (33, 34). Western blots performed on mitochondrial extracts separately confirmed an increase in PINK1 mitochondrial localization in LGK974-treated cells (Figure 3C). This increase was inversely correlated with reduced mitochondrial mass as measured on a whole cell level by a reduction in TOM20 (Figure 3D–E), suggesting LGK974 leads to stabilization of PINK1 on mitochondria and increased mitophagy. Additionally, there appeared to be a qualitative difference in the co-localization of TOM20 and LC3 based on whole cell imaging (Figure 3E), an observation compatible with an induction of mitophagy by LGK974.

PORCNi impairs cellular bioenergetics and mitochondrial metabolism in *RNF43*-mutant PDAC

Prolonged opening of mPTP can lead to MMP dissipation and uncoupling of oxidative phosphorylation, resulting in increased ATP hydrolysis and disruption of redox homeostasis. ATP levels were decreased on a per cell basis in *RNF43*-mutant PDAC following LGK974 (Figure 4A), which was phenocopied by *WNT7B* knockdown (Figure 4B, Supplemental Figure 4E). Knockdown of *CTNNB1* inhibited ATP levels to a lesser extent (Figure 4B) despite similarly inhibiting WNT/β-catenin transcriptional activity based on the endogenous target gene *AXIN2* (Supplemental Figure 4E). These data suggest PORCNi decreases ATP production in *RNF43*-mutant PDAC through a mechanism that is partially independent and upstream of effects on β-catenin stabilization and transcriptional activity.

The metabolic basis for reduced ATP with LGK974 was further examined in Seahorse assays. LGK974 reduced oxygen consumption rates (OCR) and extracellular acidification rates (ECAR) at 24 and 72 hours without significantly altering their ratios (Figure 4C, Supplemental Figure 6A–B). Supporting its inhibitory action on oxidative phosphorylation, LGK974 inhibited cell viability and ATP production to a similar extent when the glycolytic pathway was suppressed by replacing glucose in media with galactose or a low concentration of glucose (Supplemental Figure 6F–G). As reduced mitochondrial content could alone explain OCR differences, mitochondria were isolated from treated cells and functionally evaluated in mitochondrial Seahorse assays. LGK974 reduced substrate utilization by electron transport chain (ETC) Complexes I and II. This reduction in function correlated with a decrease in proteins from Complex I and Complex II compared to other ETC complexes (Figure 4D–E). Thus, LGK974 was found to inhibit oxidative phosphorylation through reductions in mitochondrial content and its disruption of ETC complex I and II protein levels and function on a per mitochondria basis.

LGK974 effects on the tricarboxylic acid (TCA) cycle were explored by stable isotope-resolved metabolomics with uniform 1, D-glucose [U^{13}-C6] labeling. LGK974 decreased the total and labeled pools of most TCA metabolites, as well as amino acids and nucleotides linked to TCA cycle (Figure 4F–H, Supplemental Figure 6C–D, Supplemental Table 4). While the labeled pool of acetyl-CoA was decreased, labeled pyruvate and lactate were not significantly altered. Likewise, while total levels of most glycolytic intermediates were decreased, labeled pools of these glycolytic intermediates were not significantly altered. Direct metabolic footprint analysis of extracellular media at 48 and 96 hours revealed a reduction in lactate production in line with ECAR measurements, but with an increase in glucose consumption at 96 hours (Supplemental Figure 6C). Glutamine consumption was unchanged based on footprint analysis, while a non-significant trend towards reduced glutamate production was noted at 96 hours (Supplemental Figure 6C). Together, these results may indicate LGK974 alters the balance of lactate transport across the plasma membrane and/or flux through the glycolytic pathway. Indeed, LGK974 reduced total and labeled pools of key pentose phosphate pathway (PPP) and hexosamine biosynthesis pathway (HBP) intermediates, including ribulose-5-P, ribose-5-phosphate, and UDP-N-acetylglucosamine (Figure 4H, Supplemental Figure 6E). Thus, PORCNi appears to alter utilization of glucose-derived carbons in the TCA cycle and glycolytic pathway.

Therapeutically leveraging PORCNi-induced metabolic adaptations

Autophagic processes were noted be an enriched term in RNA-seq analysis with LGK974 (Figure 1). Autophagy associated GO terms were also enriched in the aforementioned publicly available RNA-seq dataset of orthotopic HPAF-II tumors treated with ETC-159 (3) (Supplemental Figure 7A), extending this observation to the *in vivo* setting. LGK974 increased autophagy in *RNF43*-mutant cell lines as measured by mCherry-GFP sensor fused to LC3 (dual green and red fluorescence in autophagosome, red fluorescence in autolysosome) with enhanced mCherry expression (Figure 5A). LGK974 also increased lysosomal acidification (Figure 5B), which was reversed upon addition of exogenous Wnt3a (Figure 5C). LGK974 increased LC3-II by western blot in AsPC-1 cell lysates in both fed and serum/glucose-starved conditions, which was confirmed to represent an increase in autophagic flux based on further accumulation of LC3-II with bafilomycin (Figure 5D). Similar results were observed in HPAF-II and Capan-2 (Supplemental Figure 7B). Speculating autophagy may serve as a compensatory response to mitochondrial and metabolic stress, we examined if LGK974 sensitized tumor cell lines to chloroquine, a widely used inhibitor of autophagy. Loewe and HSA analyses confirmed dual treatment with LGK974 and chloroquine synergistically inhibited the growth of *RNF43*-mutant PDAC cell lines, but not non-transformed HPDE cells (Figure 5E–F, Supplemental Figure 7C–E).

Discussion

A multi-omic approach employed here to study the effects of PORCNi has revealed autocrine WNT ligand signaling plays a crucial role in supporting mitochondrial metabolism and homeostasis in *RNF43*-mutant PDAC. These results complement a growing body of literature on WNT signaling in cancer metabolic reprogramming and highlight how pathway-specific differences in the activation and/or inhibition of WNT will divergently

impact of aerobic glycolysis and/or oxidative phosphorylation in different genetic contexts (3, 35–40). LGK974 was found to increase the levels of active GSK3β specifically in mitochondria, a potential mechanism by which PORCNi may exert potent and specific growth antagonism in *RNF43*-mutant PDAC or other WNT ligand-addicted cancers (Figure 6).

WNT is known to transcriptionally regulate mitochondrial biogenesis (36, 39) and was shown here to exert further post-transcriptional control over mitochondrial function and homeostasis in *RNF43*-mutant PDAC. PORCNi increased active GSK3β in mitochondria where it is known to regulate the activity and localization of multiple target substrates, including those linked to mitochondrial biogenesis, TCA cycle, and electron transport chain activity (26, 27, 41, 42). In cardiac myocytes, active GSK3β enhances adenine nucleotide translocator (ANT) complex formation to sensitize the mPTP. Conversely, inactive GSK3β (P-GSK3β-Ser9) blocks ANT complex formation with CyP-D to desensitize the mPTP (25, 32). Multiple oncogenic signaling pathways (e.g. AKT and ERK1/2) are thought to promote MMP by phosphorylating GSK3β on serine 9 (43). In addition to a previously described mechanism in which autocrine WNT ligand signaling sequesters GSK3β in LRP6 signalosomes (17, 18), we now highlight its action in inhibiting GSK3β mitochondrial localization and activity that presumably raises mPTP threshold to promote MMP in *RNF43*-mutant PDAC. Conversely, by increasing active mitochondrial GSK3β, PORCNi promotes pore transition, mitochondrial membrane depolarization, and clearance of damaged mitochondria by PINK1-mediated mitophagy.

RNF43 is a tumor suppressor gene whose loss has been linked to growth dependency on WNT ligand signaling (44–46). Data here links this growth dependency to control of ATP production through mitochondrial respiration and differ from a prior study in colon cancer that showed inhibition of WNT signaling with dominant-negative TCF4 or XAV939 blocks aerobic glycolysis and increases mitochondrial respiration through a mechanism involving PDK1 and pyruvate flux (37). Results presented here are not necessarily discordant, as LGK974 did block glycolysis, possibly by the same β-catenin-dependent transcriptional mechanism. In contrast to dnTCF4 in colon cancer, LGK974 blocked mitochondrial respiration. Importantly, dominant-negative TCF4 and XAV939 inhibit WNT below the level at which GSK3β localization and activity is impacted by WNT ligand signaling. Thus, cancer metabolic phenotypes would appear to be heavily influenced by the specific mechanism and level at which the WNT pathway is dysregulated and therapeutically targeted.

Preclinical/clinical studies with PORCNi and other agents targeting the WNT pathway at or above the level of ligand-receptor interaction point to potential issues with acquired resistance and on-target clinical toxicities, including dysgeusia and disrupted bone homeostasis and pathologic fractures (9, 47). These concerns warrant a more detailed mechanistic understanding of the biochemical and phenotypic actions of these agents. Four PORCNi are currently in Phase I clinical trials of unselected solid tumors either alone and/or in combination with other therapies. A recently reported Phase I study of single agent LGK974 showed limited activity against unselected solid tumors and some reduction in the size of the limited number of RNF43-mutant tumors evaluated (16). A clinical trial

of malignancies with predicted dependencies on WNT ligands, including RNF43-mutant PDAC, is ongoing (NCT01351103). LGK974 and ETC-159 are the most widely described PORCNi in the literature and are the subject of multiple clinical trials (3, 10, 11, 16, 48). They share a common mechanism of action of docking the PORCN catalytic site and similar potency (IC_{50}= 0.4 nM and 2.9 nM, respectively), specificity, and pharmacodynamics/kinetic properties (13, 49). Transcriptomic analysis of LGK974 here significantly overlapped with previously published *in vitro* and *in vivo* temporal transcriptomic analysis of *RNF43*-mutant PDAC with ETC-159 (3). Both datasets reveal compensatory activation and/or de-repression of oncogenic signaling pathways, including JAK/STAT, MAPK, JNK, and PPAR signaling. Madan and colleagues have also shown combinations of ETC-159 with MEK or PI3K/mTOR inhibitors synergistically inhibit the growth of *RNF43*-mutant PDAC (38). We are now exploring whether these synergistic effects could be related to their further influence on GSK3β levels and activity in mitochondria or other cellular sub-compartments. In addition to shifting signaling activity, LGK974 induced autophagy and lysosomal activity in *RNF43*-mutant PDAC. This induction appears to be an adaptive response to mitochondrial and energetic stress, as LGK974 sensitized *RNF43*-mutant PDAC cell lines to the autophagy inhibitor chloroquine. While chloroquine and hydroxychloroquine have been extensively evaluated in pre-clinical models and clinical trials in multiple cancer types including PDAC (50–54), it remains to be determined whether targeting autophagy in combination with PORCN inhibition is an effective *in vivo* strategy for targeting WNT ligand-addicted PDAC while also avoiding on-target toxicities associated with inhibiting WNT in normal tissues.

In conclusion, autocrine WNT ligand signaling regulates cellular growth and metabolism in *RNF43*-mutant PDAC through both transcriptional and post-transcriptional effects linked to mitochondrial homeostasis and function. Cellular and metabolic adaptations to mitochondrial stress and metabolic dysfunction induced by PORCNi are potential targetable vulnerabilities that warrant further investigation as combinatorial approaches for the improved treatment of WNT-addicted malignancies.

Supplementary Material

Refer to Web version on PubMed Central for supplementary material.

Acknowledgements:

KYA was supported by Ruth L. Kirschstein Institutional National Research Service Award T32 CA009056 (UCLA Tumor Biology Training Grant). DWD was supported by the Hirshberg Foundation for Pancreatic Cancer Research and P01 CA236585. DWD, TML, and CGR were supported by R01CA260678. We acknowledge the following UCLA core facilities: Metabolomics, Flow Cytometry, Mitochondrial and Metabolism, and Technology Center for Genomics and Biology.

Abbreviations list

AD	Anchorage dependent
AI	Anchorage independent
ANT	Adenine nucleotide translocator

BafA	Bafilomycin A
CCCP	Carbonyl cyanide 3-chlorophenylhydrazone
CM	Conditioned media
CsA	Cyclosporin A
CTL	Control
CyP-D	Cyclophilin-D
ECAR	Extracellular acidification rate
ECL	Enhanced chemiluminescence
ETC	Electron transport chain
FZD	Frizzled
GEO	Gene expression omnibus
GO	Gene ontology
GSEA	Gene set enrichment analysis
GSK3β	Glycogen synthase kinase 3 beta
HBP	Hexosamine biosynthesis pathway
LGK	LGK974
LRP5/6	Low-density lipoprotein-receptor related protein 5/6
MIDA	Metabolic mass isotopomer distribution analysis
MMP	Mitochondrial membrane potential
mPTP	Mitochondrial permeability transition pore
OCR	Oxygen consumption rate
OMM	Outer mitochondrial membrane
PDAC	Pancreatic ductal adenocarcinoma
PORCN	Porcupine
PPP	Pentose phosphate pathway
RNF43	Ring finger protein 43
SILAC	Stable isotope labeling by amino acids in cell culture
TCA	Tricarboxylic acid
TMRM	Tetramethylrhodamine methyl ester perchlorate

References

1. Ying H, Dey P, Yao W, Kimmelman AC, Draetta GF, Maitra A, et al. Genetics and biology of pancreatic ductal adenocarcinoma. Genes Dev. 2016;30(4):355–85. [PubMed: 26883357]
2. Donahue TR, Dawson DW. Leveraging Mechanisms Governing Pancreatic Tumorigenesis To Reduce Pancreatic Cancer Mortality. Trends Endocrinol Metab. 2016;27(11):770–81. [PubMed: 27461042]
3. Madan B, Harmston N, Nallan G, Montoya A, Faull P, Petretto E, et al. Temporal dynamics of Wnt-dependent transcriptome reveal an oncogenic Wnt/MYC/ribosome axis. J Clin Invest. 2018;128(12):5620–33. [PubMed: 30300142]
4. Arensman MD, Kovochich AN, Kulikauskas RM, Lay AR, Yang PT, Li X, et al. WNT7B mediates autocrine Wnt/beta-catenin signaling and anchorage-independent growth in pancreatic adenocarcinoma. Oncogene. 2014;33(7):899–908. [PubMed: 23416978]
5. Pasca di Magliano M, Biankin AV, Heiser PW, Cano DA, Gutierrez PJ, Deramaudt T, et al. Common activation of canonical Wnt signaling in pancreatic adenocarcinoma. PLoS One. 2007;2(11):e1155. [PubMed: 17982507]
6. Morris JPt, Wang SC, Hebrok M. KRAS, Hedgehog, Wnt and the twisted developmental biology of pancreatic ductal adenocarcinoma. Nat Rev Cancer. 2010;10(10):683–95. [PubMed: 20814421]
7. White BD, Chien AJ, Dawson DW. Dysregulation of Wnt/beta-catenin signaling in gastrointestinal cancers. Gastroenterology. 2012;142(2):219–32. [PubMed: 22155636]
8. Nusse R, Clevers H. Wnt/beta-Catenin Signaling, Disease, and Emerging Therapeutic Modalities. Cell. 2017;169(6):985–99. [PubMed: 28575679]
9. Aguilera KY, Dawson DW. WNT Ligand Dependencies in Pancreatic Cancer. Frontiers in Cell and Developmental Biology. 2021;9:1027.
10. Jiang X, Hao HX, Growney JD, Woolfenden S, Bottiglio C, Ng N, et al. Inactivating mutations of RNF43 confer Wnt dependency in pancreatic ductal adenocarcinoma. Proc Natl Acad Sci U S A. 2013;110(31):12649–54. [PubMed: 23847203]
11. Liu J, Pan S, Hsieh MH, Ng N, Sun F, Wang T, et al. Targeting Wnt-driven cancer through the inhibition of Porcupine by LGK974. Proc Natl Acad Sci U S A. 2013;110(50):20224–9. [PubMed: 24277854]
12. Madan B, Ke Z, Harmston N, Ho SY, Frois AO, Alam J, et al. Wnt addiction of genetically defined cancers reversed by PORCN inhibition. Oncogene. 2016;35(17):2197–207. [PubMed: 26257057]
13. Yu J, Liao PJ, Xu W, Jones JR, Everman DB, Flanagan-Steet H, et al. Structural model of PORCN illuminates disease-associated variants and drug binding sites. bioRxiv. 2021:2021.07.19.452875.
14. Yu J, Liao PJ, Xu W, Jones JR, Everman DB, Flanagan-Steet H, et al. Structural model of PORCN illuminates disease-associated variants and drug binding sites. J Cell Sci. 2021.
15. Shah K, Panchal S, Patel B. Porcupine inhibitors: Novel and emerging anti-cancer therapeutics targeting the Wnt signaling pathway. Pharmacol Res. 2021;167:105532. [PubMed: 33677106]
16. Rodon J, Argiles G, Connolly RM, Vaishampayan U, de Jonge M, Garralda E, et al. Phase 1 study of single-agent WNT974, a first-in-class Porcupine inhibitor, in patients with advanced solid tumours. Br J Cancer. 2021;125(1):28–37. [PubMed: 33941878]
17. Taelman VF, Dobrowolski R, Plouhinec JL, Fuentealba LC, Vorwald PP, Gumper I, et al. Wnt signaling requires sequestration of glycogen synthase kinase 3 inside multivesicular endosomes. Cell. 2010;143(7):1136–48. [PubMed: 21183076]
18. Bilic J, Huang YL, Davidson G, Zimmermann T, Cruciat CM, Bienz M, et al. Wnt induces LRP6 signalosomes and promotes dishevelled-dependent LRP6 phosphorylation. Science. 2007;316(5831):1619–22. [PubMed: 17569865]
19. Ding L, Billadeau DD. Glycogen synthase kinase-3beta: a novel therapeutic target for pancreatic cancer. Expert Opin Ther Targets. 2020;24(5):417–26. [PubMed: 32178549]
20. Rose S, Frye RE, Slattery J, Wynne R, Tippett M, Pavliv O, et al. Oxidative stress induces mitochondrial dysfunction in a subset of autism lymphoblastoid cell lines in a well-matched case control cohort. PLoS One. 2014;9(1):e85436. [PubMed: 24416410]

21. Kaiser P, Wohlschlegel J. Identification of ubiquitination sites and determination of ubiquitin-chain architectures by mass spectrometry. Methods Enzymol. 2005;399:266–77. [PubMed: 16338362]
22. Zheng S, Tang J. synergyfinder: Calculate and Visualize Synergy Scores for Drug Combinations 2021 2021.
23. Steinhart Z, Pavlovic Z, Chandrashekhar M, Hart T, Wang X, Zhang X, et al. Genome-wide CRISPR screens reveal a Wnt-FZD5 signaling circuit as a druggable vulnerability of RNF43-mutant pancreatic tumors. Nat Med. 2017;23(1):60–8. [PubMed: 27869803]
24. Correia SC, Santos RX, Perry G, Zhu X, Moreira PI, Smith MA. Mitochondrial importance in Alzheimer's, Huntington's and Parkinson's diseases. Adv Exp Med Biol. 2012;724:205–21. [PubMed: 22411245]
25. Zorov DB, Juhaszova M, Yaniv Y, Nuss HB, Wang S, Sollott SJ. Regulation and pharmacology of the mitochondrial permeability transition pore. Cardiovasc Res. 2009;83(2):213–25. [PubMed: 19447775]
26. Chiara F, Rasola A. GSK-3 and mitochondria in cancer cells. Front Oncol. 2013;3:16. [PubMed: 23386998]
27. Yang K, Chen Z, Gao J, Shi W, Li L, Jiang S, et al. The Key Roles of GSK-3beta in Regulating Mitochondrial Activity. Cell Physiol Biochem. 2017;44(4):1445–59. [PubMed: 29190615]
28. Beurel E, Grieco SF, Jope RS. Glycogen synthase kinase-3 (GSK3): regulation, actions, and diseases. Pharmacol Ther. 2015;148:114–31. [PubMed: 25435019]
29. Bijur GN, Jope RS. Glycogen synthase kinase-3 beta is highly activated in nuclei and mitochondria. Neuroreport. 2003;14(18):2415–9. [PubMed: 14663202]
30. King TD, Bijur GN, Jope RS. Caspase-3 activation induced by inhibition of mitochondrial complex I is facilitated by glycogen synthase kinase-3beta and attenuated by lithium. Brain Res. 2001;919(1):106–14. [PubMed: 11689167]
31. Metcalfe C, Bienz M. Inhibition of GSK3 by Wnt signalling--two contrasting models. J Cell Sci. 2011;124(Pt 21):3537–44. [PubMed: 22083140]
32. Juhaszova M, Zorov DB, Yaniv Y, Nuss HB, Wang S, Sollott SJ. Role of glycogen synthase kinase-3beta in cardioprotection. Circ Res. 2009;104(11):1240–52. [PubMed: 19498210]
33. Ge P, Dawson VL, Dawson TM. PINK1 and Parkin mitochondrial quality control: a source of regional vulnerability in Parkinson's disease. Mol Neurodegener. 2020;15(1):20. [PubMed: 32169097]
34. Ashrafi G, Schwarz TL. The pathways of mitophagy for quality control and clearance of mitochondria. Cell Death Differ. 2013;20(1):31–42. [PubMed: 22743996]
35. Morrish F, Hockenbery D. MYC and mitochondrial biogenesis. Cold Spring Harb Perspect Med. 2014;4(5).
36. Sherwood V WNT signaling: an emerging mediator of cancer cell metabolism? Mol Cell Biol. 2015;35(1):2–10. [PubMed: 25348713]
37. Pate KT, Stringari C, Sprowl-Tanio S, Wang K, TeSlaa T, Hoverter NP, et al. Wnt signaling directs a metabolic program of glycolysis and angiogenesis in colon cancer. EMBO J. 2014;33(13):1454–73. [PubMed: 24825347]
38. Zhong Z, Sepramaniam S, Chew XH, Wood K, Lee MA, Madan B, et al. PORCN inhibition synergizes with PI3K/mTOR inhibition in Wnt-addicted cancers. Oncogene. 2019;38(40):6662–77. [PubMed: 31391551]
39. Rasmussen ML, Ortolano NA, Romero-Morales AI, Gama V. Wnt Signaling and Its Impact on Mitochondrial and Cell Cycle Dynamics in Pluripotent Stem Cells. Genes (Basel). 2018;9(2).
40. Mo Y, Wang Y, Zhang L, Yang L, Zhou M, Li X, et al. The role of Wnt signaling pathway in tumor metabolic reprogramming. J Cancer. 2019;10(16):3789–97. [PubMed: 31333796]
41. Xu R, Hu Q, Ma Q, Liu C, Wang G. The protease Omi regulates mitochondrial biogenesis through the GSK3beta/PGC-1alpha pathway. Cell Death Dis. 2014;5:e1373. [PubMed: 25118933]
42. Juhaszova M, Zorov DB, Kim SH, Pepe S, Fu Q, Fishbein KW, et al. Glycogen synthase kinase-3beta mediates convergence of protection signaling to inhibit the mitochondrial permeability transition pore. J Clin Invest. 2004;113(11):1535–49. [PubMed: 15173880]

43. Hausenloy DJ, Yellon DM. Reperfusion injury salvage kinase signalling: taking a RISK for cardioprotection. Heart Fail Rev. 2007;12(3–4):217–34. [PubMed: 17541822]
44. Kinde I, Bettegowda C, Wang Y, Wu J, Agrawal N, Shih Ie M, et al. Evaluation of DNA from the Papanicolaou test to detect ovarian and endometrial cancers. Sci Transl Med. 2013;5(167):167ra4.
45. Ryland GL, Hunter SM, Doyle MA, Rowley SM, Christie M, Allan PE, et al. RNF43 is a tumour suppressor gene mutated in mucinous tumours of the ovary. J Pathol. 2013;229(3):469–76. [PubMed: 23096461]
46. Ong CK, Subimerb C, Pairojkul C, Wongkham S, Cutcutache I, Yu W, et al. Exome sequencing of liver fluke-associated cholangiocarcinoma. Nat Genet. 2012;44(6):690–3. [PubMed: 22561520]
47. Ram Makena M, Gatla H, Verlekar D, Sukhavasi S, M KP, K CP. Wnt/beta-Catenin Signaling: The Culprit in Pancreatic Carcinogenesis and Therapeutic Resistance. Int J Mol Sci. 2019;20(17).
48. Hao HX, Jiang X, Cong F. Control of Wnt Receptor Turnover by R-spondin-ZNRF3/RNF43 Signaling Module and Its Dysregulation in Cancer. Cancers (Basel). 2016;8(6).
49. Poulsen A, Ho SY, Wang W, Alam J, Jeyaraj DA, Ang SH, et al. Pharmacophore Model for Wnt/Porcupine Inhibitors and Its Use in Drug Design. J Chem Inf Model. 2015;55(7):1435–48. [PubMed: 26024410]
50. Chude CI, Amaravadi RK. Targeting Autophagy in Cancer: Update on Clinical Trials and Novel Inhibitors. Int J Mol Sci. 2017;18(6).
51. Verbaanderd C, Maes H, Schaaf MB, Sukhatme VP, Pantziarka P, Sukhatme V, et al. Repurposing Drugs in Oncology (ReDO)-chloroquine and hydroxychloroquine as anti-cancer agents. Ecancermedicalscience. 2017;11:781. [PubMed: 29225688]
52. Yang S, Wang X, Contino G, Liesa M, Sahin E, Ying H, et al. Pancreatic cancers require autophagy for tumor growth. Genes Dev. 2011;25(7):717–29. [PubMed: 21406549]
53. Maycotte P, Gearheart CM, Barnard R, Aryal S, Mulcahy Levy JM, Fosmire SP, et al. STAT3-mediated autophagy dependence identifies subtypes of breast cancer where autophagy inhibition can be efficacious. Cancer Res. 2014;74(9):2579–90. [PubMed: 24590058]
54. Boone BA, Bahary N, Zureikat AH, Moser AJ, Normolle DP, Wu WC, et al. Safety and Biologic Response of Pre-operative Autophagy Inhibition in Combination with Gemcitabine in Patients with Pancreatic Adenocarcinoma. Ann Surg Oncol. 2015;22(13):4402–10. [PubMed: 25905586]
55. PubChem Compound Summary for CID 46926973 [Internet].

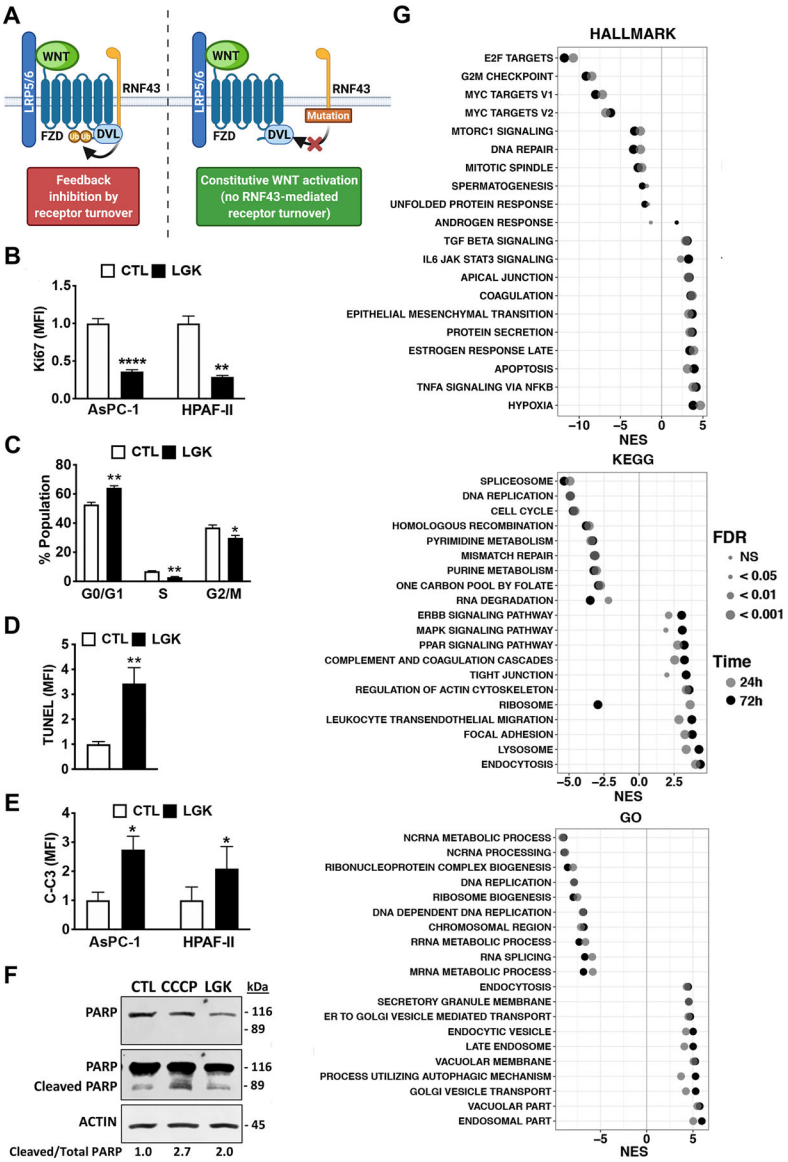

Figure 1: LGK974 inhibits *RNF43*-mutant PDAC viability with accompanying transcriptional alterations.

(A) Inactivating mutations in *RNF43* result in loss of FZD receptor turnover and constitutive WNT ligand signaling activity. Schematic created with Biorender.com. AsPC-1 treated for 48H with LGK974 (LGK), carbonyl cyanide 3-chlorophenylhydrazone (CCCP), and/or vehicle control (CTL) were assessed by (B) Ki67 immunofluorescence, (C) propidium iodide (PI) flow cytometry, (D) TUNEL staining, (E) cleaved caspase 3 (C-C3) immunofluorescence, and (F) total and cleaved PARP by immunoblot (short and long exposures presented). (G) Top RNA-seq based Hallmark, KEGG, and GO terms enriched with LGK974 in AsPC-1 (FDR <0.0001). Statistics: see Materials and Methods.

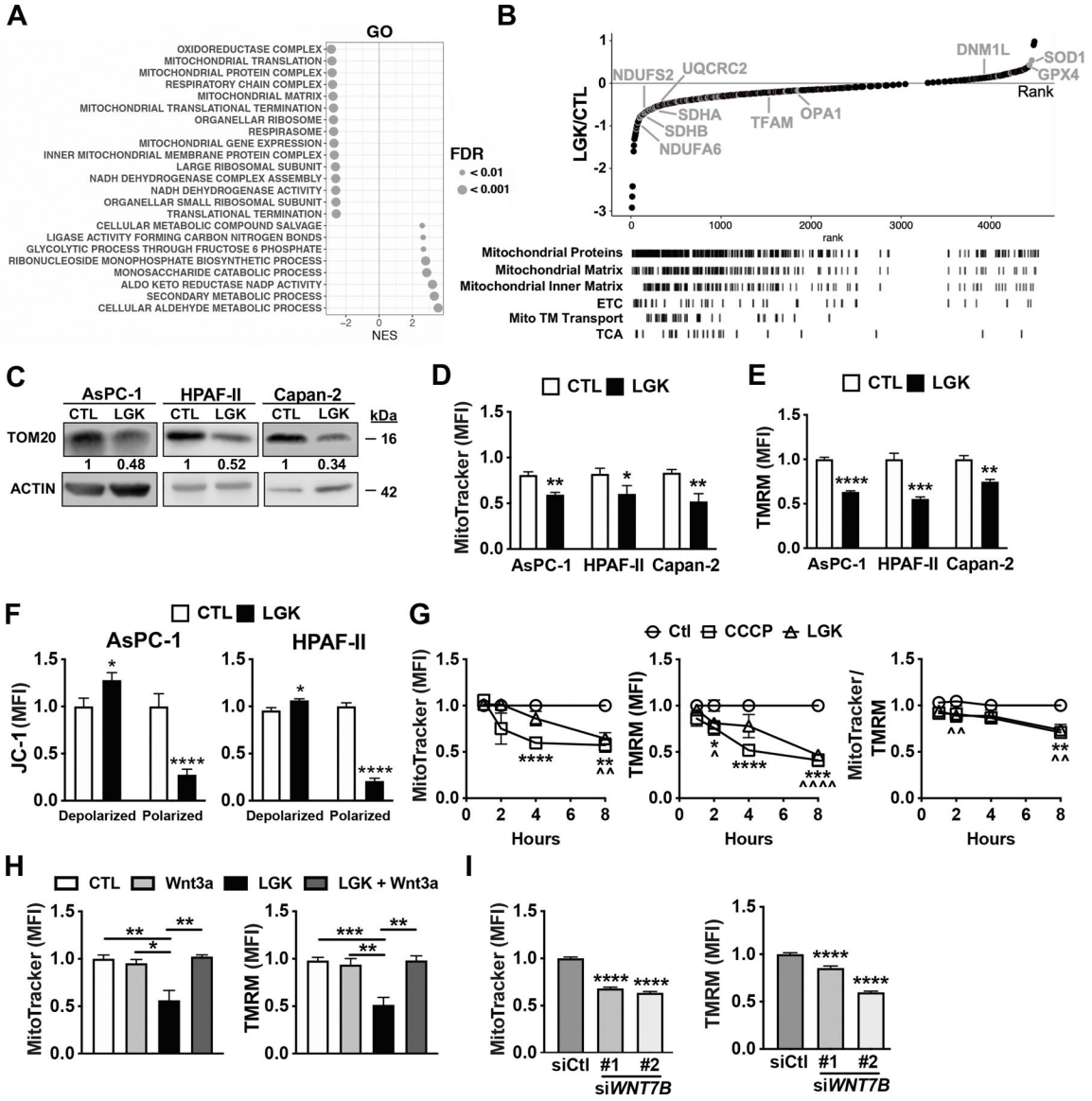

Figure 2: LGK974 disrupts mitochondrial homeostasis in *RNF43*-mutant PDAC.

Global protein quantification by SILAC for AsPC-1 for LGK974 (LGK) versus control (CTL) treatments at 8H showing (A) top GO terms and (B) distribution of mitochondrial proteins (gray) and associated mitochondrial GO terms (FDR <0.0001). (C) Western blots for TOM20 and ACTIN (loading control) on whole cell lysates (WCL). (D) MitoTracker Green, (E) TMRM, and (F) JC-1 immunofluorescence of *RNF43*-mutant PDAC lines at 24H. MitoTracker Green and TMRM of AsPC-1 comparing (G) LGK974 or 10 μM CCCP (* LGK vs CTL; ^ CCCP vs CTL). (H) LGK974 ± Wnt3a CM at 24H. (I) *WNT7B* siRNA knockdown at 48H. Statistics: see Materials and Methods.

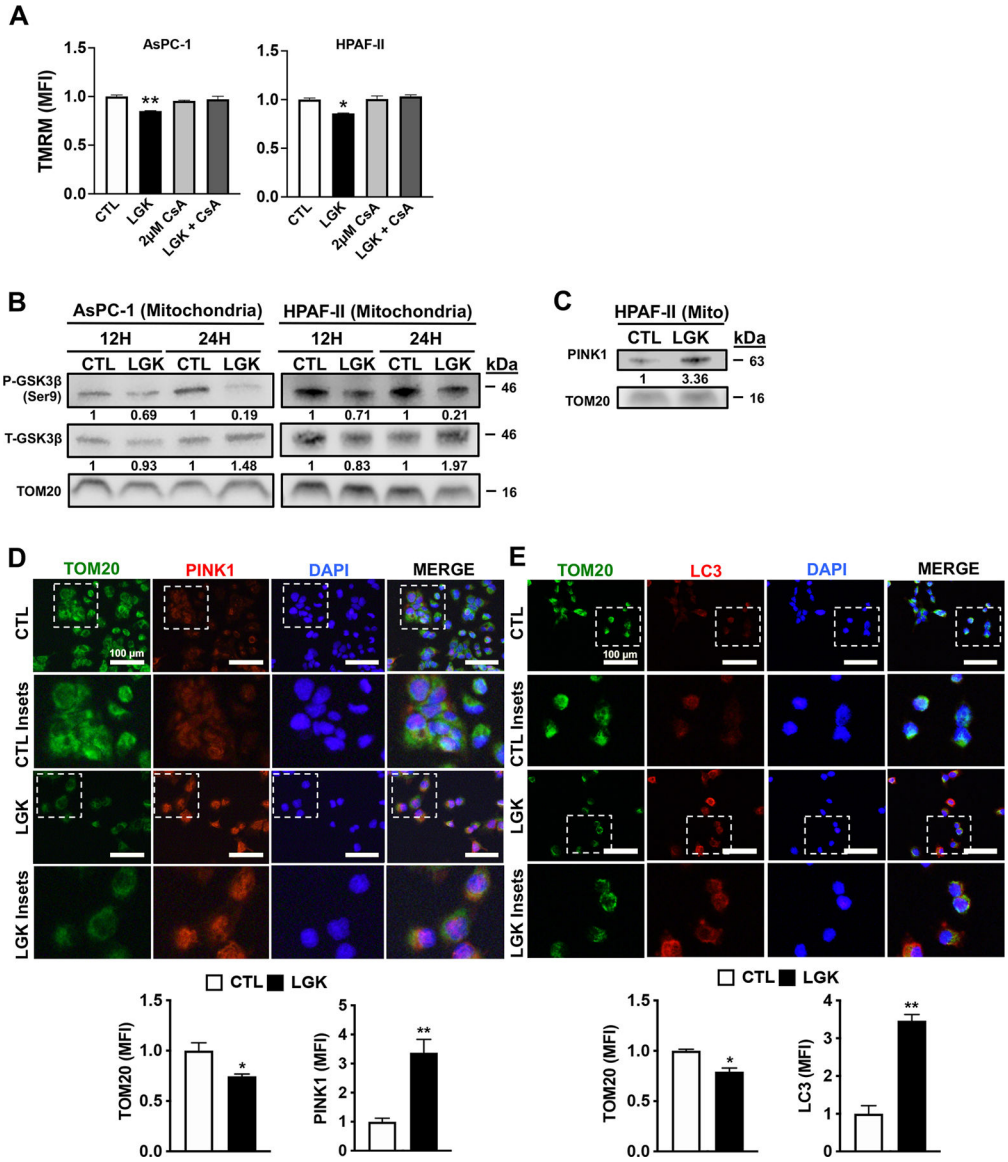

Figure 3: LGK974 function is linked to mitochondrial permeability transition pore and mitochondrial damage.

(A) MMP based on TMRM immunofluorescence with LGK974 (LGK) ± cyclosporin A (CsA, 2 μM) measured at 12H. Western blots on (B-C) isolated mitochondrial (mito) extracts derived from LGK974 (LGK) or vehicle (CTL) treated cells where TOM20 serves as a loading control for equivalent mitochondrial protein. (D-E) AsPC-1 immunofluorescence images and quantification on a whole cell level for mitochondrial content (TOM20), mitochondrial damage (PINK1), and autophagy machinery (LC3) measured at 48H. Statistics: see Materials and Methods.

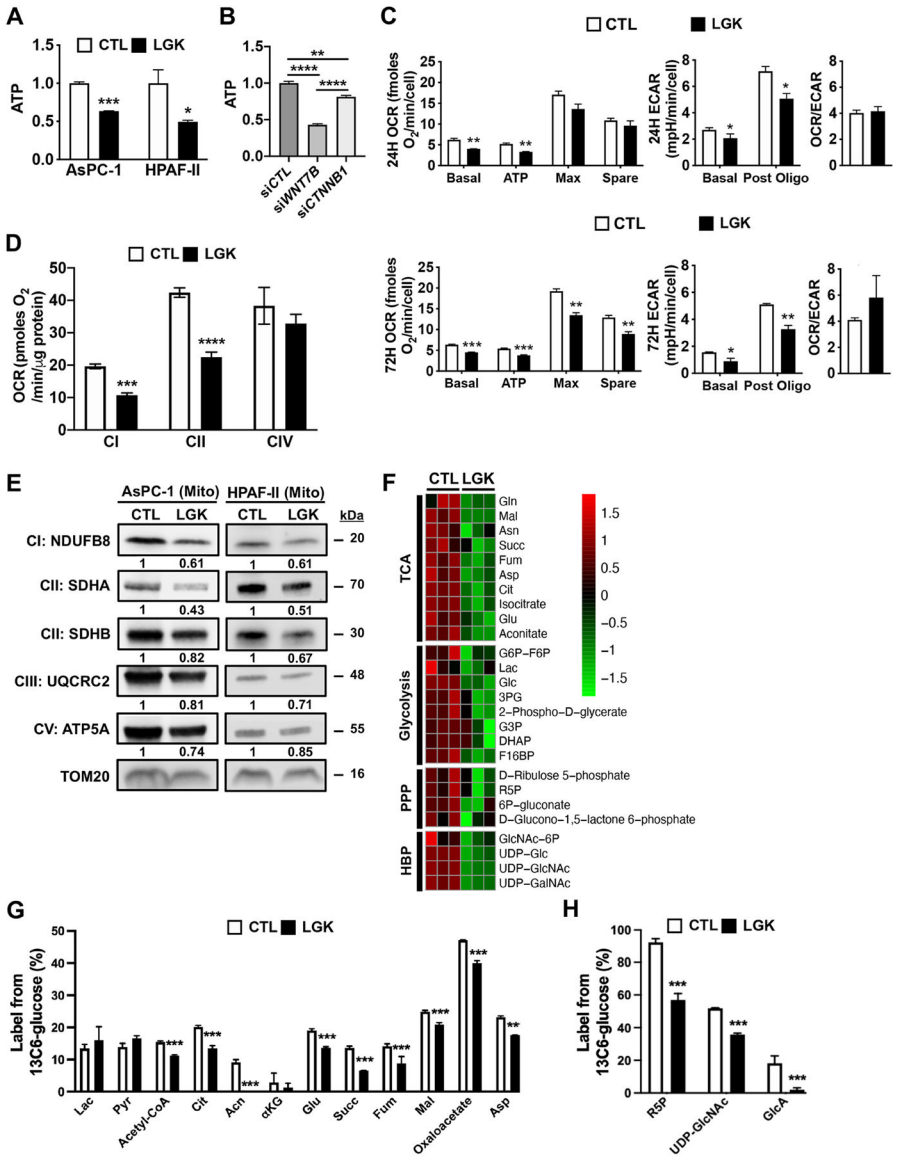

Figure 4: LGK974 inhibits mitochondrial metabolism and electron transport chain activity.

ATP levels following (A) LGK974 (LGK) or vehicle (CTL) at 24H or (B) siRNA knockdown of *WNT7B* or *CTNNB1* in AsPC-1 at 48H. (C) Seahorse analysis of treated AsPC-1 cells at 24 and 72H. (D) Substrate utilization by ETC complex measured by Seahorse analysis of viable mitochondria isolated from AsPC-1 at 72H treatment. (E) Western blots for ETC proteins in mitochondrial (mito) extracts from cells treated for 72H. 1, D-glucose [U^{13}-C6] stable isotope labeling and LC-MS/MS analysis of AsPC-1 cells treated for 36H showing (F) relative levels of selected significantly altered metabolites ($p<0.05$, z-score converted values) and (G-H) isotopomer distribution of labeled glucose in indicated metabolites. Statistics: see Materials and Methods.

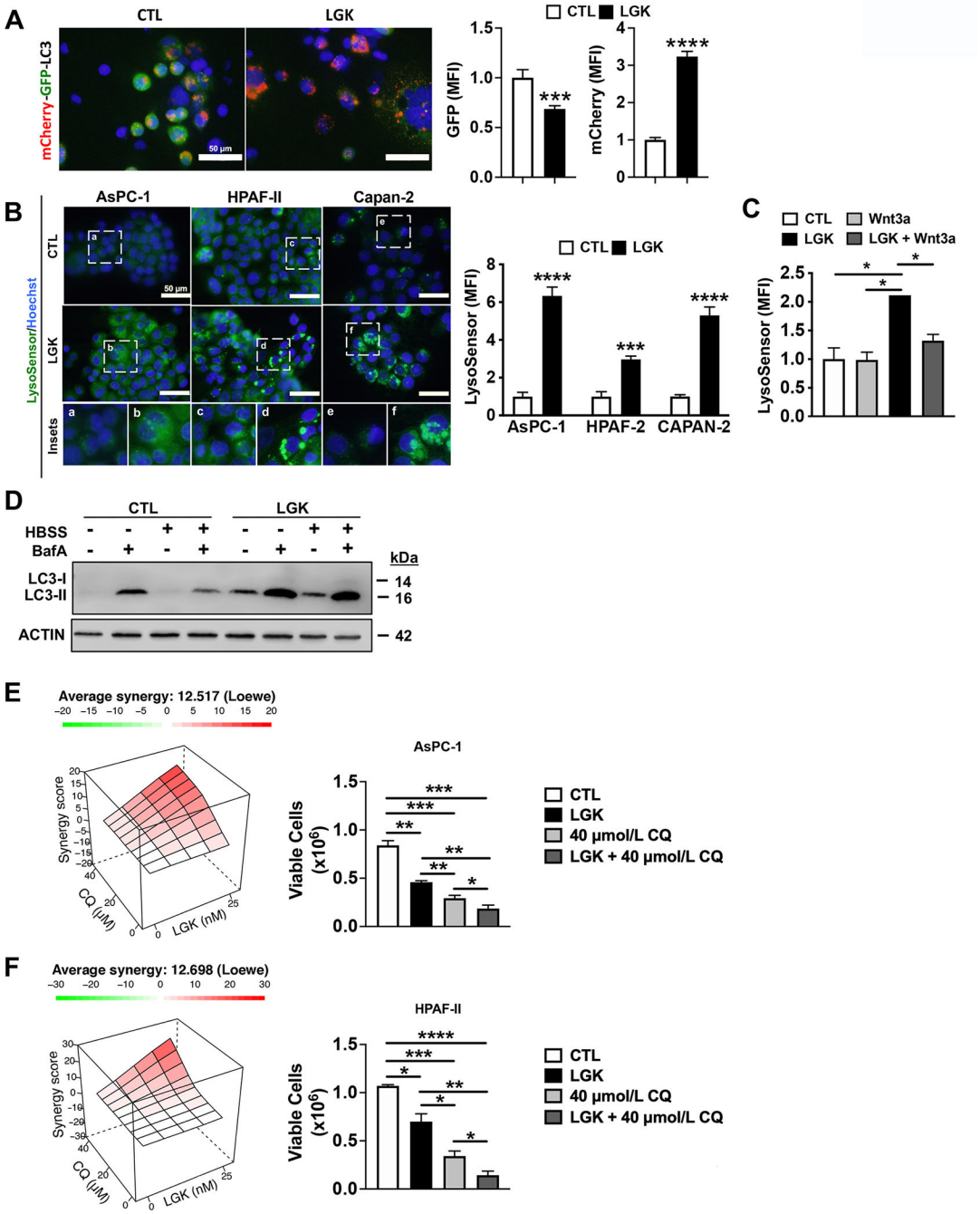

Figure 5: Macroautophagy and mitophagy are induced in response to LGK974.

(A) Immunofluorescence images and quantification of free autophagosomes (GFP and mCherry) and autophagosomes fused with the lysosome (mCherry only) for LGK974 (LGK) and vehicle control (CTL) treated AsPC-1 at 24H. (B) Immunofluorescence images and quantification of lysosomal acidification (LysoSensor Green) at 24H and (C) LysoSensor Green measures of AsPC-1 with LGK974 ± Wnt3a CM. (D) Western blots of whole cell lysates (WCL) from AsPC-1 at 24 hours control or LGK974, followed by 3 hours ± starvation in HEPES buffered saline solution (HBSS) and/or ± bafilomycin A (BafA).

Loewe synergy analyses of cell viability for indicated LGK974 ± chloroquine treatment combinations after 72H determined in (E) AsPC-1 and (F) HPAF-II based on PI-negative cell counts. Statistics: see Materials and Methods.

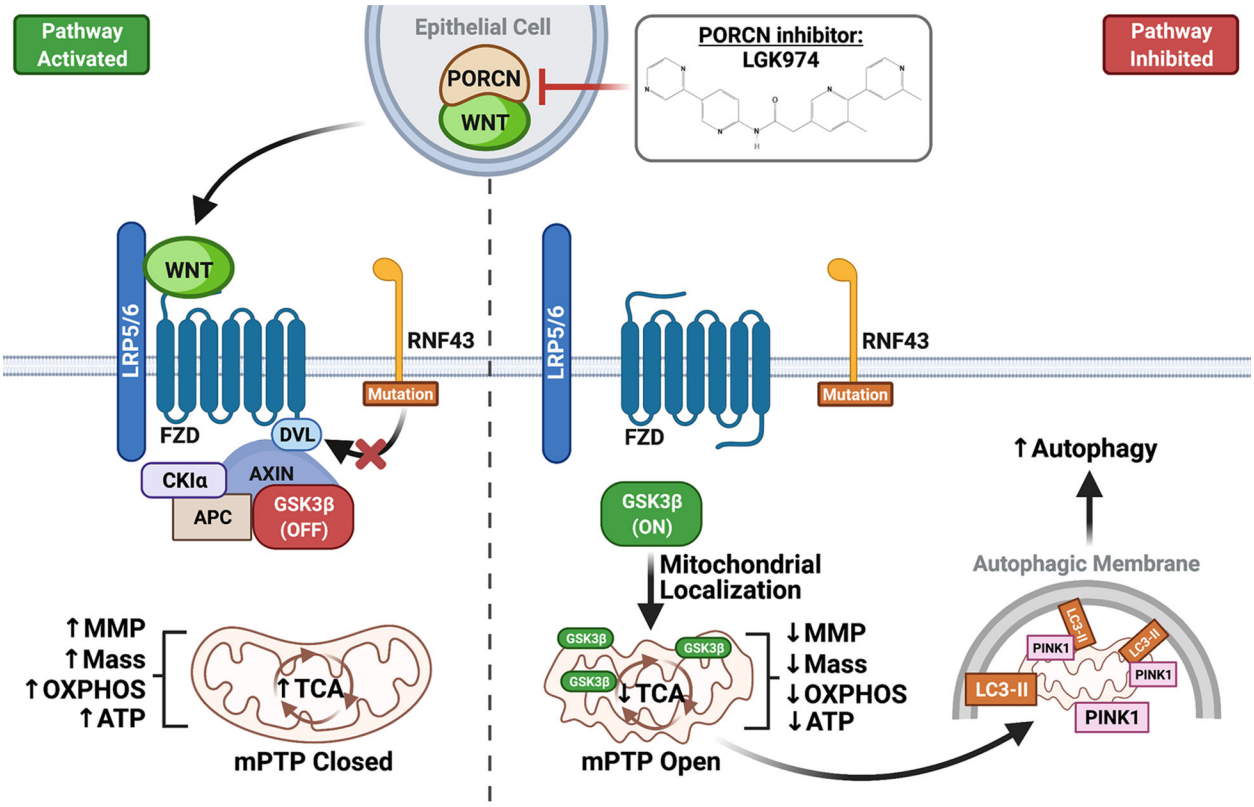

Figure 6: PORCNi disrupts mitochondrial function and homeostasis.

(Left panel) *RNF43* mutation potentiates constitutive WNT ligand signaling that inhibits GSK3β and alters its localization. (Right panel) PORCNi by LGK974 (chemical structure from (55)) increases levels of active GSK3β in mitochondria and results in disrupted mitochondrial membrane potential (MMP), function, and dynamics. Damaged mitochondria recruit autophagy machinery for mitochondrial clearance/quality control. Created with BioRender.com.